



# High-voltage aqueous planar symmetric sodium ion micro-batteries with superior performance at low-temperature of $-40\text{ }^{\circ}\text{C}$

Xiao Wang<sup>a,d</sup>, Huijuan Huang<sup>b</sup>, Feng Zhou<sup>a</sup>, Prattek Das<sup>a,d</sup>, Pengchao Wen<sup>a</sup>,  
Shuanghao Zheng<sup>a,c</sup>, Pengfei Lu<sup>a</sup>, Yan Yu<sup>b,c,\*</sup>, Zhong-Shuai Wu<sup>a,c,\*</sup>

<sup>a</sup> State Key Laboratory of Catalysis, Dalian Institute of Chemical Physics, Chinese Academy of Sciences, Dalian 116023, China

<sup>b</sup> Hefei National Laboratory for Physical Sciences at the Microscale, Department of Materials Science and Engineering, CAS Key Laboratory of Materials for Energy Conversion, University of Science and Technology of China, University of Chinese Academy of Sciences, Hefei, Anhui 230026, China

<sup>c</sup> Dalian National Laboratory for Clean Energy, Chinese Academy of Sciences, Dalian 116023, China

<sup>d</sup> University of Chinese Academy of Sciences, Beijing 100049, China

## ARTICLE INFO

### Keywords:

High voltage  
Water-in-salt electrolyte  
Symmetric  
Planar  
Sodium ion micro-batteries  
Low temperature

## ABSTRACT

Aqueous sodium ion micro-batteries (ANIMBs) hold great promise in smart wearable microelectronics due to the abundant reserves, low cost and high safety of sodium. However, their applications are substantially hindered by the narrow electrochemical stability window of aqueous electrolytes within a limited temperature range. Herein, we report a prototype of high-voltage planar ANIMBs based on symmetric interdigital microelectrodes working in water-in-salt (WiS) electrolyte (17 M NaClO<sub>4</sub>) and displaying exceptional performance at low temperature. This work features nanoflower Na<sub>3</sub>V<sub>2</sub>(PO<sub>4</sub>)<sub>3</sub> (NVP)-based electrodes with perfectly matched voltage range as both anode and cathode in the WiS electrolyte operating in a widened electrochemical stability window (2.7 V vs. Na<sup>+</sup>/Na) under ultralow freezing point of  $-50\text{ }^{\circ}\text{C}$ . The resulting ANIMBs with interdigital in-plane geometry deliver remarkable volumetric capacity of 45 mAh/cm<sup>3</sup> and energy density of 77 mWh/cm<sup>3</sup>, which are superior to most reported sodium-based micropower sources. Notably, the NVP||NaClO<sub>4</sub>||NVP micro-batteries exhibit a high coulombic efficiency of > 99% at room temperature down to  $-40\text{ }^{\circ}\text{C}$ . Furthermore, the NVP||NaClO<sub>4</sub>||NVP ANIMBs present admirable flexibility and modular integration. We believe that our ANIMBs can potentially enjoy wide market adoption ranging from domestic appliances to safe intelligent wearable microelectronics, especially those applications that need to be operated below freezing temperature.

## 1. Introduction

The ever-increasing consumer demands for wearable and smart miniaturized integrated electronics, microscale electrochemical energy storage devices has unleashed a new era of competition for self-powered microsystems [1–7]. Traditional electrochemical energy storage devices that are limited by heavy weight, large volume and fixed shape have failed to fit the specific needs of the smart and integrated electronics technology when miniaturization and lightweight have become the priority in system design [8]. Therefore, micro-batteries and micro-supercapacitors are emerging as potential micropower suppliers for smart and integrated electronics. Among them, micro-supercapacitors are lower in energy densities ( $< 5\text{ mWh/cm}^3$ ) [9, 10], making them less appealing to certain applications. This performance gap can be filled by micro-batteries [11,12], especially lithium

ion micro-batteries. Although immense progress has been witnessed in lithium ion micro-batteries over the past decade, their applications are marred by unresolved issues such as the scarcity and high price of lithium resources along with the use of flammable and toxic organic electrolytes [13].

Moving towards aqueous Na ion micro-batteries (ANIMBs) could be the solution to these issues due to the use of safe aqueous electrolyte, high abundance, low cost of sodium resources and low standard redox potential ( $-2.71\text{ V}$  vs. standard hydrogen electrode) [14,15]. However, the narrow electrochemical stability window of traditional aqueous electrolyte (up to 1.23 V) has inevitably become the bottleneck in the selection of electrode materials. Recently, high concentration aqueous electrolyte was proposed as an effective approach to extend the voltage window of water-based electrolyte system [16–20], but still preserve the intrinsic properties of traditional aqueous electrolytes (e.g., low

\* Corresponding author at:Dalian National Laboratory for Clean Energy, Chinese Academy of Sciences, Dalian 116023, China

E-mail addresses: [yanyumse@ustc.edu.cn](mailto:yanyumse@ustc.edu.cn) (Y. Yu), [wuzs@dicp.ac.cn](mailto:wuzs@dicp.ac.cn) (Z.-S. Wu).

<https://doi.org/10.1016/j.nanoen.2020.105688>

Received 4 October 2020; Received in revised form 7 December 2020; Accepted 9 December 2020

Available online 18 December 2020

2211-2855/© 2020 Elsevier Ltd. All rights reserved.

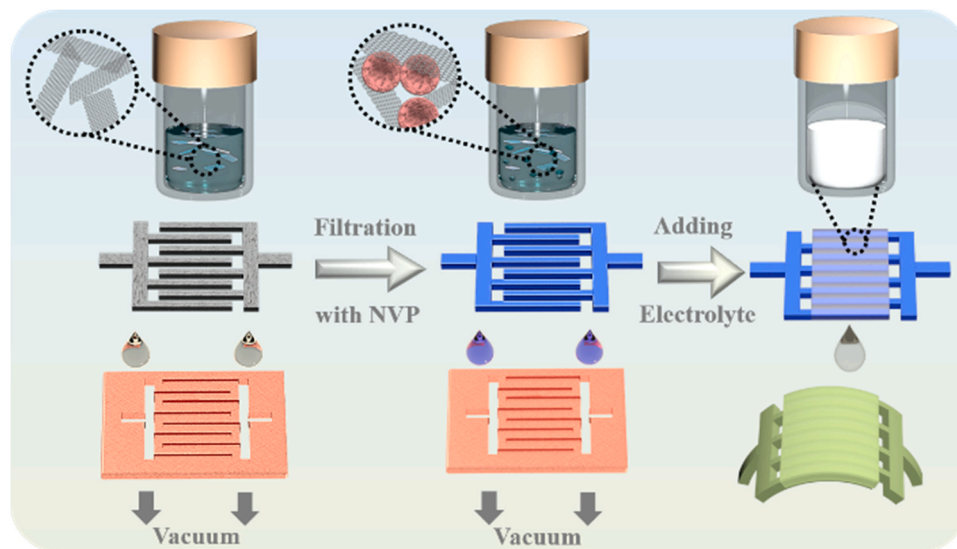


Fig. 1. Schematic illustration of the fabrication of the symmetric planar NVP||NaClO<sub>4</sub>||NVP ANIMBs.

flammability, low solvent activity, high chemical stability that suppresses side reactions) [21–24]. When it comes to low temperature operation, high concentration aqueous electrolytes still show sufficient ionic conductivity and counteract the freezing problem of most aqueous electrolytes [25]. Meanwhile, researchers have also been trying to find the next leap forward in ANIMBs by searching for suitable electrode materials. So far, numerous electrode materials, including layered transition metal oxides [26–29], Prussian blue analogs [30], carbon-based organic materials [31] and polyanionic compounds [32], have shown promising performance for sodium ion batteries in the traditional stacked geometry. Among them, Na<sub>3</sub>V<sub>2</sub>(PO<sub>4</sub>)<sub>3</sub> (NVP) presents intriguing advantages such as remarkable energy density (400 Wh/kg), superior sodium diffusion ability, high ionic conductivity, impressive structural and thermal stability [27,33]. Nevertheless, high-voltage aqueous planar ANIMBs working at low temperature range have not yet been reported, due to the lack of electrolyte that is cost-efficient and can operate at high voltage along with electrochemically active yet stable electrode materials.

In this work, a prototype of high-voltage aqueous planar interdigital ANIMBs with high energy density and low-temperature performance was successfully constructed using high concentration electrolyte (17 M NaClO<sub>4</sub>) and nanoflower NVP as both anode and cathode on a single substrate. Multiple factors work together to realize fast electron and ion transfer in the electrode: (1) high ionic conductivity of electrolyte; (2) highly conductive carbon layer coated on NVP; (3) high electronic conductivity of exfoliated graphene (EG) as current collector. Therefore, the separator-free ANIMBs possess high voltage window up to 2.3 V, high capacity of 45 mAh/cm<sup>3</sup> at 0.03 mA/cm<sup>2</sup> under room temperature and excellent capacity retention of 88% after 1000 cycles at room temperature. Remarkably, at substantially low temperature of –40 °C, 88% retention of capacity obtained at room-temperature can still be retained with high coulombic efficiency over multiple cycles. The exceptional performances could be ascribed to a significant decrease in the number of free water molecules in the highly concentrated WiS electrolyte [25]. Furthermore, the as-prepared NVP||NaClO<sub>4</sub>||NVP ANIMBs exhibit not only remarkable energy density of 77 mWh/cm<sup>3</sup> and power density of 769 W/cm<sup>3</sup>, but also outstanding flexibility without capacity degradation under different bending states, and impressive series and parallel integration to readily boost the capacity and voltage output.

## 2. Experiment

### 2.1. Synthesis of NVP nanoflower

The nanoflower NVP was synthesized by high temperature annealing according to the previous literature [27]. Firstly, 0.72 g vanadium pentoxide (V<sub>2</sub>O<sub>5</sub>) and 1.52 g oxalic acid dehydrate (C<sub>2</sub>H<sub>2</sub>O<sub>4</sub>·2H<sub>2</sub>O) were put into 40 mL de-ionized water (H<sub>2</sub>O) using 70 °C water bath in round-bottomed flask and stirring for 1 h. Then, 1.84 g sodium carbonate (NaH<sub>2</sub>PO<sub>4</sub>·2H<sub>2</sub>O) and 0.4 g glucose (C<sub>6</sub>H<sub>12</sub>O<sub>6</sub>) were poured into the above solution and stirred for 10 min. Finally, 100 mL *n*-propanol was added to the mixture under continuous stirring for 30 min. After the mixture dried in 70 °C oven overnight, the NVP was obtained.

### 2.2. Fabrication of planar NVP||NaClO<sub>4</sub>||NVP ANIMBs

The construction of planar ANIMBs was based on mask-assisted filtration we developed [34,35], involving the sequential filtration of high-quality EG ethanol dispersion (1 mL, 0.1 mg/mL), NVP dispersion (1 mL, 0.5 mg/mL, 10 wt% EG) on cathode side and NVP dispersion on anode side (1.5 mL, 0.5 mg/mL, 10 wt% EG). The resulting microelectrodes with eight fingers (length of 14 mm, width of 1 mm, interspace of 0.5 mm, active area of 63%, Fig. S1) was successfully constructed on a nylon membrane (0.22 μm, Agela Technologies). After removing the mask and adding the electrolyte (e.g., 17 M NaClO<sub>4</sub>), the planar NVP||NaClO<sub>4</sub>||NVP ANIMBs were achieved.

### 2.3. Preparation of highly concentrated electrolytes

17 M NaClO<sub>4</sub> was diluted in distilled water to obtain the highly concentrated electrolyte, and then the silica fumed powder (0.5 g) was added into the above solution (6 mL). Other aqueous electrolytes (8.4 M NaTFSI, 1.3 M Na<sub>2</sub>SO<sub>4</sub>) were prepared using similar approach.

## 3. Results and discussion

The fabrication process of aqueous symmetric planar NVP||NaClO<sub>4</sub>||NVP ANIMBs is schematically illustrated in Fig. 1. Initially, high-quality EG nanosheets (Fig. S2) were synthesized by electrochemical exfoliation [36], and directly filtrated on the nylon membrane to construct highly conductive network of planar interdigital microelectrodes that are free of both separator and metal current collector. Then, the symmetric microelectrodes were constructed by sequential deposition of NVP

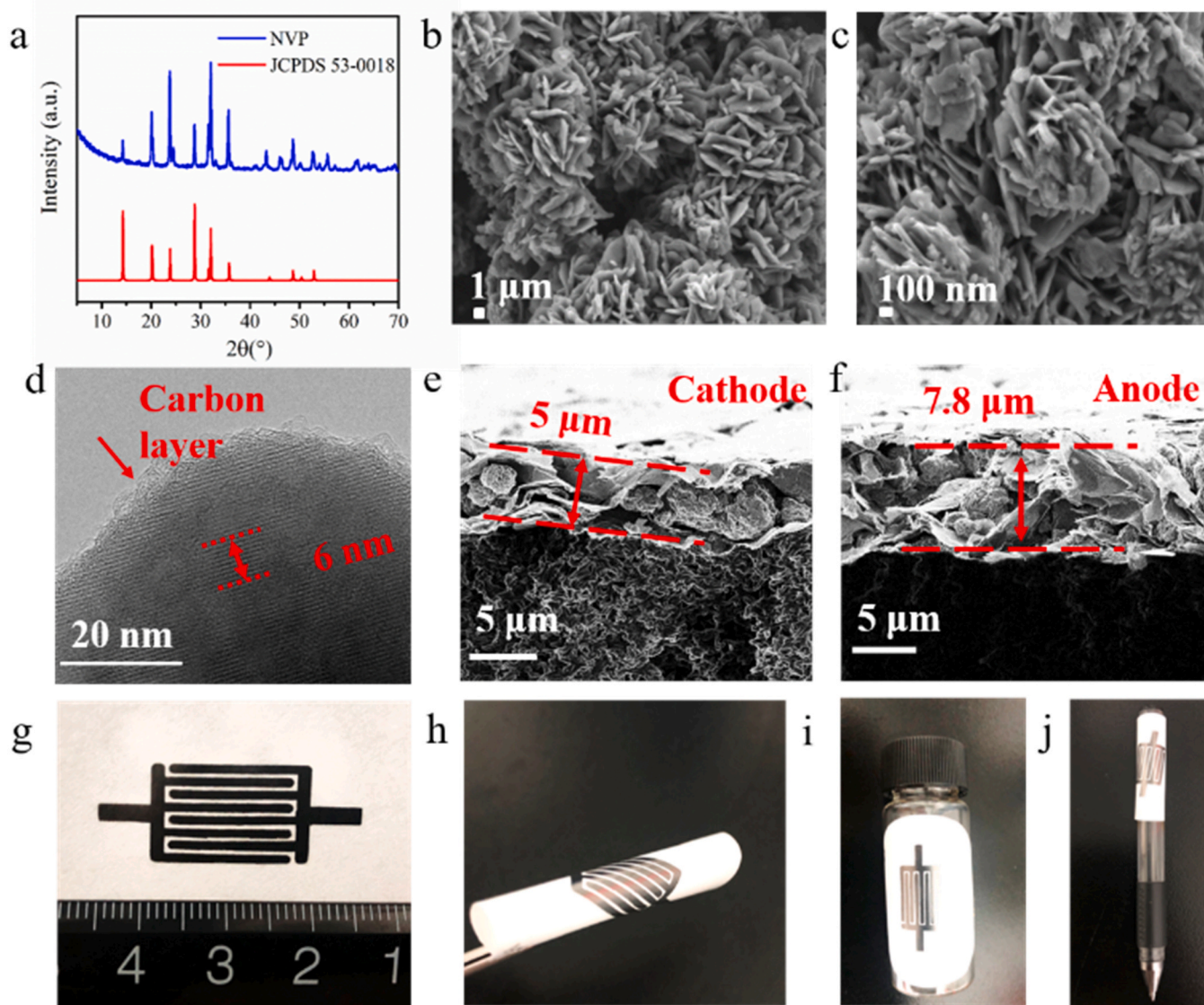


**Fig. 2.** Morphology of the NVP and characterization of the cathode and anode. a–d) XRD patterns (a), SEM images in different magnifications (b and c) and HRTEM image (d) of NVP. e and f) Cross-sectional SEM images of the cathode (e) and anode (f). g–j) Optical images of the ANIMBs in the flat (g), bending states (h), and label-like tagged onto the bottle (i) and pen (j).

dispersion (0.5 mg/mL, 10 wt% EG) on each side of the mask for the assembly of anode and cathode. It is worth noting that the NVP nanoflowers were prepared by thermal annealing, resulting in not only a highly crystalline composition of thin nanosheets (34 nm) (Fig. 2a–c) [27,37], but also a thin carbon layer in about 2.5 nm (Fig. 2d, Fig. S3). After the successful material synthesis, the interdigital electrode with thicknesses of 5 and 7.8  $\mu\text{m}$  (Fig. 2e–f) were chosen for cathode and anode respectively after optimization (Fig. S4). Furthermore, the as-prepared micropatterns (Fig. 2g) demonstrated splendid flexibility without any delamination from the substrate under different extreme states, such as curved (Fig. 2h) and label-like tagged onto the bottle or pen (Fig. 2i–j, Fig. S5). Finally, the planar ANIMBs were sealed after drop-casting WiS electrolyte (17 M  $\text{NaClO}_4$  gel) on the electrode.

To attain the high-voltage NVP|| $\text{NaClO}_4$ ||NVP ANIMBs, three kinds of sodium ion-based electrolytes with different anions were exploited, including sulfate ( $\text{SO}_4^{2-}$ ), trifluoromethanesulfonimide (TFSI $^-$ ) and perchlorate ( $\text{ClO}_4^-$ ). According to the Hofmeister series that illustrates the role of salt anions in the aqueous solvation process and their water solvation strength [15], the relative capability to destabilize the bulk water molecules of these representative inorganic ions can be sorted as

follows:  $\text{SO}_4^{2-} < \text{TFSI}^- < \text{ClO}_4^-$ , which hints that  $\text{ClO}_4^-$  salts have a strong tendency to break the bulk water molecules and change solvation structures with ion aggregations. It is noteworthy that the 17 M  $\text{NaClO}_4$  WiS electrolyte possesses a relatively wide electrochemical stable window of 2.7 V, compared with NaTFSI (2.3 V) and  $\text{Na}_2\text{SO}_4$  (1.5 V) (Fig. 3a) [16], which matches well with NVP that exhibits a pair of stable redox peaks within this voltage window (Fig. S6). Furthermore, the water-structure-breaking strength of salts corresponded to the solubility of inorganic salts [38]. When reaching the solubility limits in water, the water-breaking anions that contain the high end in the rank order (i.e.,  $\text{ClO}_4^-$ ) were indicated to be capable of forming complex ion networks with the water molecules, destroying the original hydrogen bonding networks [38]. Molecular dynamics (MD) simulations further revealed the structural differences between low and high concentration electrolytes theoretically (Fig. 3b). In the less concentrated electrolyte, the formation of hydrogen bonding network by the free water molecules is responsible for the broad band as confirmed by Raman spectra. Comparatively, most of the water molecules are tightly connected with  $\text{Na}^+$  ions in the highly concentrated electrolyte. As a result, a strong hydrogen bonding network cannot be formed among the remaining free

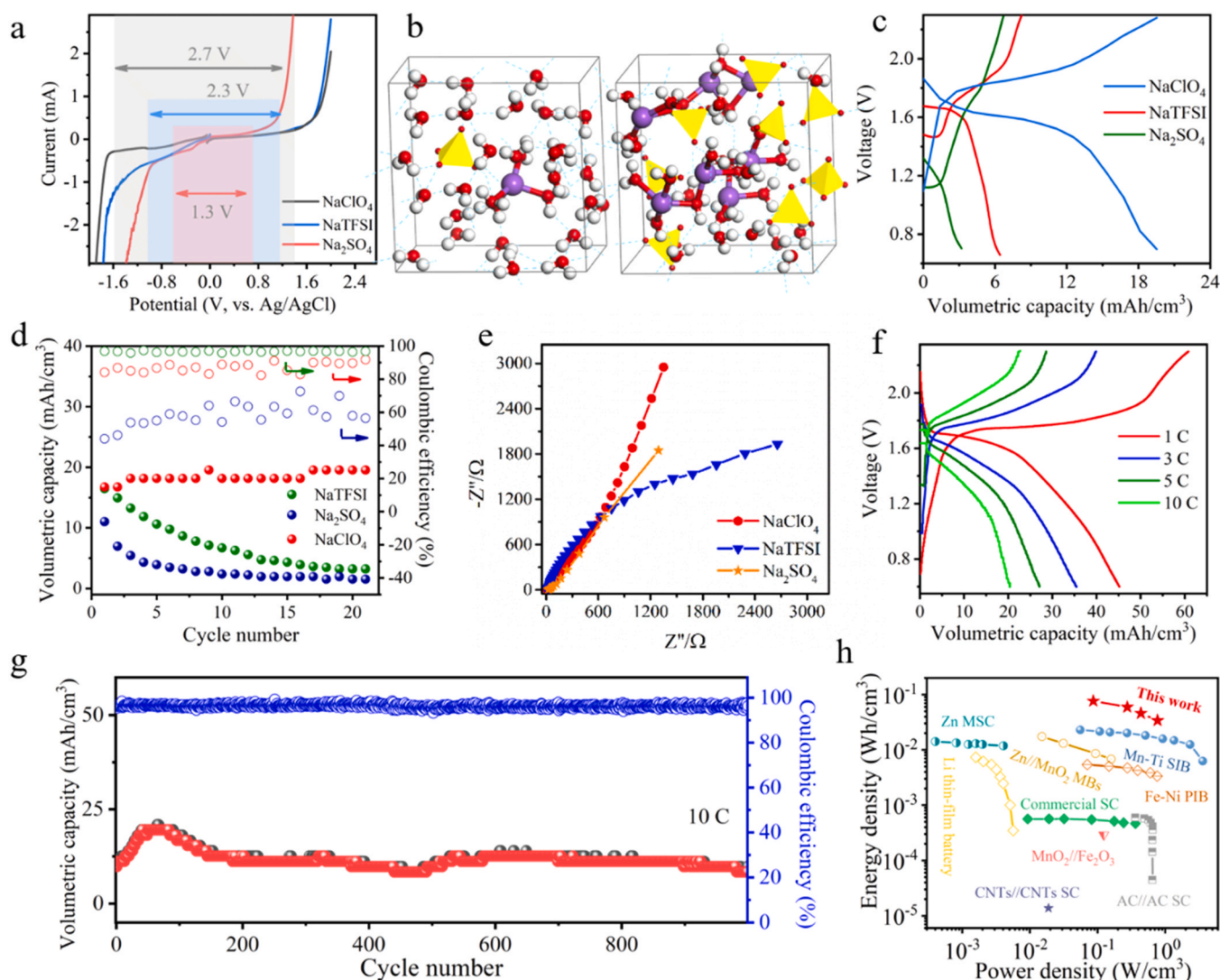


**Fig. 3.** Electrochemical performance of the symmetric planar NVP||NaClO<sub>4</sub>||NVP ANIMBs tested at room temperature. a) Overall electrochemical stability window of 17 M NaClO<sub>4</sub>, 8.4 M NaTFSI and 1.3 M Na<sub>2</sub>SO<sub>4</sub> electrolyte on the Pt electrodes at 10 mV/s. b) 1 M NaClO<sub>4</sub> and 17 M NaClO<sub>4</sub> electrolyte during MD simulations. Atom colors: Na, purple; O, red; H, white; Cl, yellow. c–e) The GCD profiles (c), cyclability (d) and EIS spectra (e) of the ANIMBs tested at different high concentrated electrolyte systems: 17 M NaClO<sub>4</sub>, 8.4 M NaTFSI and 1.3 M Na<sub>2</sub>SO<sub>4</sub>. f) The GCD profiles of the NVP||NaClO<sub>4</sub>||NVP ANIMBs obtained at different current density ranging from 0.03 to 0.3 mA/cm<sup>2</sup> (corresponding to 1–10 C). g) Long-term cyclability of the NVP||NaClO<sub>4</sub>||NVP ANIMBs measured for 1000 cycles tested at 0.3 mA/cm<sup>2</sup> (10 C). h) Ragone plot of the NVP||NaClO<sub>4</sub>||NVP ANIMBs compared with other energy storage devices. (For interpretation of the references to color in this figure legend, the reader is referred to the web version of this article.)

water molecules, contributing to a decrease in the intensity of the water molecules and broadened voltage window [39]. Furthermore, Raman spectroscopy (Fig. S7a) distinguished the fingerprints based on the changes in the solvation structure of the different electrolyte candidates. For deionized water and Na<sub>2</sub>SO<sub>4</sub>, the broad band of water clusters maintain their symmetric (near 3200 cm<sup>-1</sup>) and asymmetric (near 3400 cm<sup>-1</sup>) [40] vibration modes in water molecules well, owing to the appearance of free water in majority. By contrast, it was found that the hydration characteristics of NaClO<sub>4</sub> such as a maximum peak at 3400 cm<sup>-1</sup> and the disappearance of the shoulder peak at 3200 cm<sup>-1</sup> are obviously different from those of other traditional electrolytes and are similar to NaTFSI, implying a reduction in water activity and the formation of Na<sup>+</sup> and ClO<sub>4</sub><sup>-</sup> coordinated ions pairs. In addition, the Nyquist plots showed a higher ionic conductivity of 59 mS/cm for 17 M NaClO<sub>4</sub> WiS electrolyte compared with Na<sub>2</sub>SO<sub>4</sub> (15 mS/cm) and NaTFSI (6 mS/cm) (Fig. S7b), validating the contribution of electrolyte anion in the ionic conductivity of the electrolyte.

To evaluate the effect of the different electrolytes on electrochemical

performance, the planar ANIMBs (denoted as NVP||NaClO<sub>4</sub>||NVP, NVP||NaTFSI||NVP and NVP||Na<sub>2</sub>SO<sub>4</sub>||NVP) were fabricated with symmetric NVP microelectrodes in the WiS electrolytes of 17 M NaClO<sub>4</sub>, 8.4 M NaTFSI and 1.3 M Na<sub>2</sub>SO<sub>4</sub> respectively. In the case of NaClO<sub>4</sub> electrolyte, the ANIMBs at 0.3 mA/cm<sup>2</sup> exhibit outstanding volumetric capacity of 18 mAh/cm<sup>3</sup>, which is higher than those of 6 and 3 mAh/cm<sup>3</sup> for NaTFSI and Na<sub>2</sub>SO<sub>4</sub>, respectively (Fig. 3c), which is ascribed to the above-mentioned difference in ionic conductivities. Furthermore, the NVP||NaClO<sub>4</sub>||NVP micro-batteries present superior cyclability of 100% capacity retention after 20 cycles at 0.3 mA/cm<sup>2</sup> (Fig. 3d), in comparison with NVP||Na<sub>2</sub>SO<sub>4</sub>||NVP (21%) and NVP||NaTFSI||NVP (13%). This phenomenon could be explained by the enhanced ionic conductivity and ion diffusion of NaClO<sub>4</sub> that shows the steepest slope at the high frequency region of the electrochemical impedance spectroscopy (EIS, Fig. 3e, Fig. S8). Benefiting from high ionic conductivity, NVP||NaClO<sub>4</sub>||NVP ANIMBs display excellent rate capability, showing volumetric capacities of 45, 35, 27 and 18 mAh/cm<sup>3</sup> at 0.03, 0.09, 0.15 and 0.3 mA/cm<sup>2</sup>, respectively (Fig. 3f, Figs. S9 and S10). It is worth

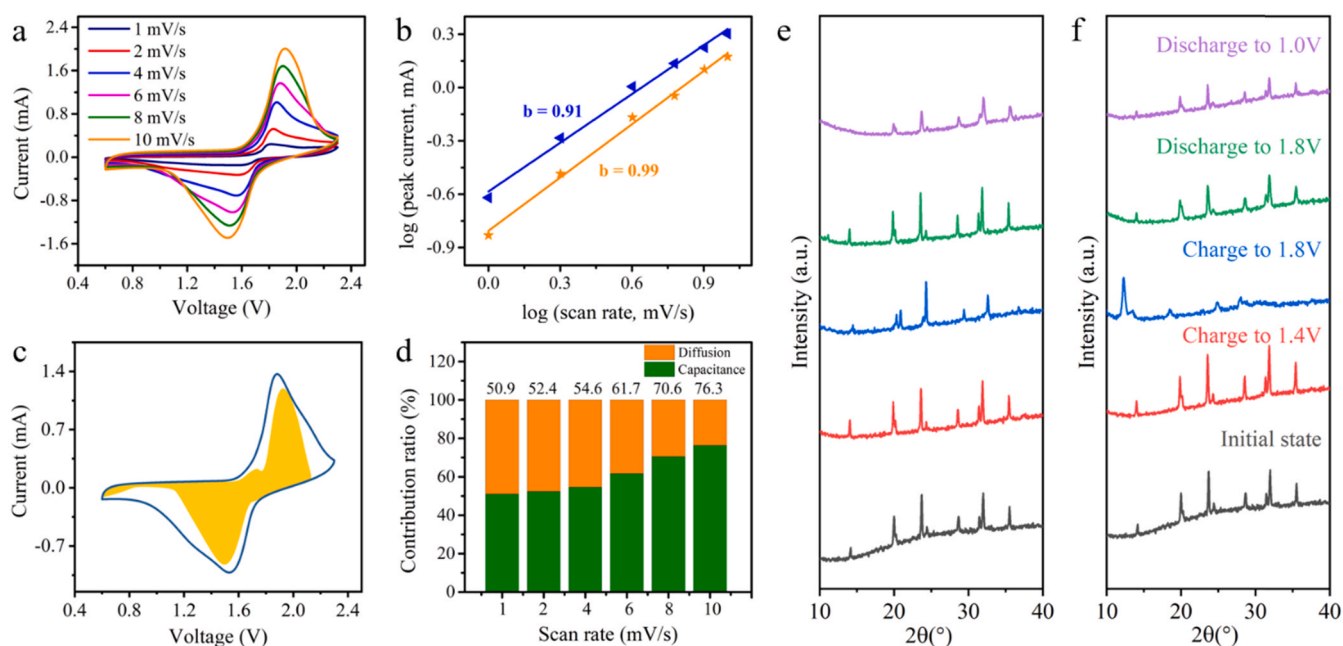


**Fig. 4.** Kinetics analysis of  $\text{Na}^+$  ion intercalation of  $\text{NVP}||\text{NaClO}_4||\text{NVP}$  ANIMBs. a) CV curves of the  $\text{NVP}||\text{NaClO}_4||\text{NVP}$  ANIMBs tested at the scan rates from 1 to 10 mV/s. b) The plots of  $\log i$  vs.  $\log v$  curves of cathodic and anodic peaks. c) Capacitive (yellow part) and diffusion-controlled capacities (void part) at 6 mV/s. d) Normalized contribution ratios of capacitive (green part) and diffusion-controlled (orange part) capacities at different scan rates. e and f) *Ex-situ* XRD patterns of the cycled NVP as cathode (e) and anode (f) in the  $\text{NVP}||\text{NaClO}_4||\text{NVP}$  ANIMB, implying the transformation of  $\text{NaV}_2(\text{PO}_4)_3$  and  $\text{Na}_5\text{V}_2(\text{PO}_4)_3$  in the cathode and anode respectively. (For interpretation of the references to color in this figure legend, the reader is referred to the web version of this article.)

noting that  $\text{NVP}||\text{NaClO}_4||\text{NVP}$  ANIMBs show long lifespan and remarkable capacity retention of 88% after 1000 cycles with average coulombic efficiency of 96% (Fig. 3g, Fig. S11). Impressively, our  $\text{NVP}||\text{NaClO}_4||\text{NVP}$  ANIMBs deliver high energy density of 77 mWh/cm<sup>3</sup> (Fig. 3h, based on the whole volume of anode and cathode) and remarkably high power density of 769 W/cm<sup>3</sup>, which is much larger than most reported batteries and supercapacitors (Table S1) [41–43].

Furthermore, the reaction kinetics of the  $\text{NVP}||\text{NaClO}_4||\text{NVP}$  was examined by cyclic voltammetry (CV). As shown in Fig. 4a, CV curves demonstrated almost overlapped redox peaks at 1.9 V and 1.5 V at scan rates from 1 to 10 mV/s (Fig. 4a), which is indicative of the sodium ion insertion and extraction. The surface capacitive and diffusion-controlled process were evaluated by the equation [44],  $i = av^b$ , where  $i$  is the current,  $v$  is scan rate, and  $a$  and  $b$  are adjustable parameters. According to the slope of the  $\log i$  vs  $\log v$  plots, it was calculated that the  $b$  values are 0.91 and 0.99 (Fig. 4b), indicating that the charge storage mechanism is dominated by surface capacitive contribution rather than the diffusion controlled process in the  $\text{NVP}||\text{NaClO}_4||\text{NVP}$ . Additionally, the capacity ratio from capacitive ( $k_1v$ ) and diffusion-controlled ( $k_2v^{1/2}$ ) process were specified based on the equation  $i = k_1v + k_2v^{1/2}$  and  $i/v^{1/2} = k_1v^{1/2} + k_2$  [45]. For example, the yellow part stands for the capacitive contribution, accounting for 61.7% of the total capacity at the scan rate of 6 mV/s (Fig. 4c). With increasing scan rates from 1 to 10 mV/s, the capacitive contribution increases from 50.9% to 71.3% (Fig. 4d). Therefore, it can be concluded that the high rate capability of the  $\text{NVP}||\text{NaClO}_4||\text{NVP}$  is the result of the predominant capacitive-controlled kinetics process. The structural evolution was examined by *ex-situ* X-ray diffraction (XRD) patterns (Fig. 4e–f), in which a two-electron reaction that involves the phase transformation between  $\text{Na}_3\text{V}_2(\text{PO}_4)_3$  and  $\text{NaV}_2(\text{PO}_4)_3$  in the cathode accompanied by the conversion of  $\text{Na}_3\text{V}_2(\text{PO}_4)_3$  to  $\text{Na}_5\text{V}_2(\text{PO}_4)_3$  in the anode takes place upon charge/discharge and the oxidation and reduction transformation of vanadium from  $\text{V}^{3+}$  up to  $\text{V}^{4+}$  and down to  $\text{V}^{2+}$  [46,47].

To meet the requirements of micropower sources in flexible electronics, the flexibility, integration and low-temperature performance of the  $\text{NVP}||\text{NaClO}_4||\text{NVP}$  ANIMBs were studied. It was observed that the

$\text{NVP}||\text{NaClO}_4||\text{NVP}$  exhibits impressive flexibility without any structural fracture at the microelectrodes under different bending states (Fig. 5a). The GCD profiles of the  $\text{NVP}||\text{NaClO}_4||\text{NVP}$  (Fig. 5b) overlap satisfactorily under bending angles from 0° to 180°, with nearly 100% capacity retention at current density of 0.6 mA/cm<sup>2</sup>. The  $\text{NVP}||\text{NaClO}_4||\text{NVP}$  micro-batteries show 93% of its original performance at 0° bending angle (Fig. 5c). Furthermore, to fulfill the requirements of integrated circuits, the integrated  $\text{NVP}||\text{NaClO}_4||\text{NVP}$  ANIMBs with high capacity and high voltage were readily prepared by parallel and serial connection (Fig. 5d). Remarkably, the  $\text{NVP}||\text{NaClO}_4||\text{NVP}$  connected in parallel from one to three cells exhibit an analogical electrochemical performance and a stepwise increase in capacity from 17, 34–60 mAh/cm<sup>3</sup> (Fig. 5e), while the output voltage remains unchanged. Moreover, the  $\text{NVP}||\text{NaClO}_4||\text{NVP}$  connected in series exhibits a stepwise increase in average discharging voltage from 1.5 V for one cell to 3 V for two cells and 4.5 V for three cells (Fig. 5f), which is demonstrative of its exceptional performance uniformity. These results are in good agreement with the decreased ESR from 20 Ω to 11 Ω and 9 Ω by increasing the number of parallel devices (Fig. S12a), while the increased ESR from 20 Ω to 37 Ω and 50 Ω by increasing the number of serial devices (Fig. S12b). Impressively, the two serially connected devices could easily light up a display screen of our institute “DICP” logo (Fig. S13a) and power a light-emitting diode (LED) under severe deformation (Fig. S13b), which is demonstrative of the great potential of integrated ANIMBs for micropower sources.

Because of the freezing of the hydrogel electrolyte at subzero temperatures, conventional aqueous electrolytes would inevitably contribute to the deterioration of performance and elasticity [48]. Differently, with an increase in the electrolyte concentration, our 17 M  $\text{NaClO}_4$  is endowed with better anti-freezing property at extremely low temperature, where superior electrochemical performance and high ion conductivity of 17 mS/cm can be achieved under −40 °C (Fig. 5g, Fig. S14). In order to validate the feasibility of 17 M  $\text{NaClO}_4$  electrolyte under low temperature, the freezing point of the electrolyte was determined by differential scanning calorimetry (DSC, Fig. S15), proving a low freezing point of −50 °C. The low freezing point is ascribed to the

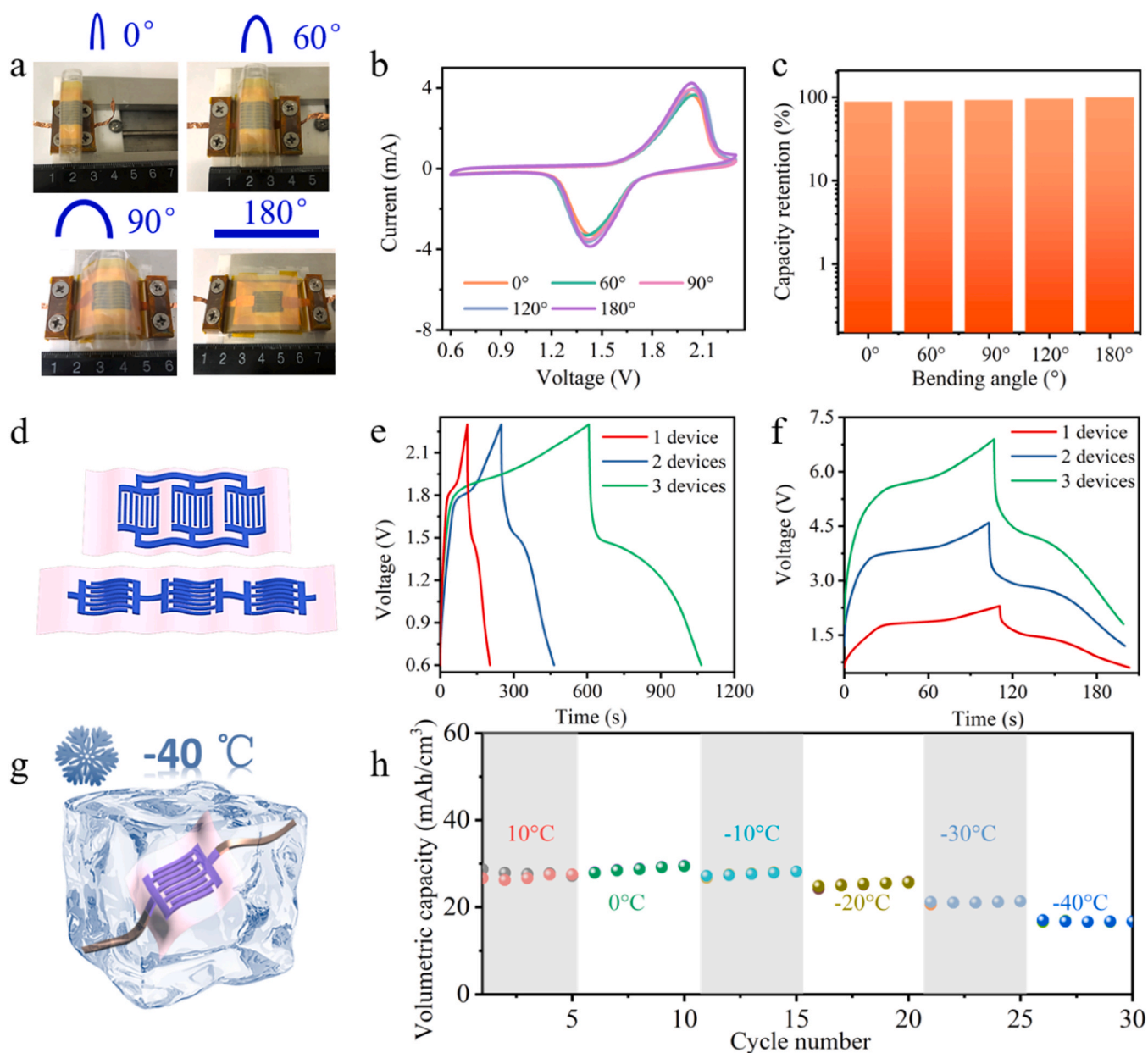


**Fig. 5.** Integration and low-temperature electrochemical performances of NVP||NaClO<sub>4</sub>||NVP ANIMBs. (a) Photographs of the NVP||NaClO<sub>4</sub>||NVP ANIMBs taken at the bending angle of 0°, 60°, 90°, 120° and 180°. (b) The corresponding CV profiles collected at 20 mV/s. (c) The capacity retention at different bending angles. (d) Schematic illustration of the integrated planar NVP||NaClO<sub>4</sub>||NVP ANIMBs connected three cells in parallel (up) and in series (bottom). (e) GCD profiles of the integrated planar NVP||NaClO<sub>4</sub>||NVP ANIMBs connected (e) in parallel and (f) in series from 1 to 3 devices. (g) Schematic illustration of the NVP||NaClO<sub>4</sub>||NVP ANIMBs at -40 °C. (h) Cyclability of the NVP||NaClO<sub>4</sub>||NVP ANIMBs measured at different temperature ranging from 10 to -40 °C at 0.3 mA/cm<sup>2</sup>.

decreased H-bonds amount in the highly soluble NaClO<sub>4</sub> where the O atoms in the water molecules are confined by the metal ions through hydration, and the high concentration in the low temperature [49]. Impressively, the NVP||NaClO<sub>4</sub>||NVP displays a high capacity of 16 mAh/cm<sup>3</sup> with a high retention of 88% under -40 °C (Fig. 5h). It is noteworthy that the NVP||NaClO<sub>4</sub>||NVP shows obvious redox peaks under -15 °C (Fig. S16), which is indicative of its superior performance under low temperature. The NVP||NaClO<sub>4</sub>||NVP shows a low equivalent series resistance (ESR) value of 27 Ω (Fig. S17) with a high capacity retention of 91% after 600 cycles (Fig. S18).

#### 4. Conclusions

In conclusion, we have successfully constructed symmetric NVP||NaClO<sub>4</sub>||NVP ANIMBs based on double-duty NVP microelectrodes and

high concentrated WiS electrolyte of 17 M NaClO<sub>4</sub>. Attributed to the synergistic effect of the high capacity NVP and the low freezing point of the highly concentrated NaClO<sub>4</sub> electrolyte, the prepared NVP||NaClO<sub>4</sub>||NVP exhibits high voltage window of 2.3 V, high energy density of 77 mWh/cm<sup>3</sup> and extraordinary stable performance at -40 °C. In particular, the development of planar sodium ion micro-batteries with highly concentrated electrolyte not only wean us off the dependence on lithium resources, but also provides a new avenue to improve the capacity and output voltage and simplify the electrode manufacturing process through the design of symmetric microelectrode. Therefore, this work provides new insights from several aspects. Specifically, the full utilization of low-cost high concentrated WiS is beneficial for obtaining high-performance sodium ion micro-batteries with enhanced safety features under low temperature, which holds great potential to be applied safely in wearable microelectronics even in harsh environments.

### CRedit authorship contribution statement

**Xiao Wang:** Materials preparation and Characterization, Methodology, Data curation, Writing- Original draft preparation. **Huijuan Huang:** Materials preparation and Writing. **Feng Zhou:** Materials preparation. **Prateek Das:** Data collection and Writing. **Pengchao Wen:** Materials preparation. **Shuanghao Zheng:** Formal analysis. **Pengfei Lu:** Writing and MD simulations. **Yan Yu:** Conceptualization, Writing- Reviewing and Editing. **Zhong-Shuai Wu:** Conceptualization, Writing- Reviewing and Editing.

### Declaration of Competing Interest

The authors declare that they have no known competing financial interests or personal relationships that could have appeared to influence the work reported in this paper.

### Acknowledgments

The authors acknowledge the financial support from National Key R&D Program of China (Grants 2016YFB0100100, and 2016YFA0200200), National Natural Science Foundation of China (Grants 51872283, 21805273, 51872277, U1910210 and 51925207, 22075279, 22005297, 22005298), Liaoning BaiQianWan Talents Program, LiaoNing Revitalization Talents Program (Grant XLYC1807153), Natural Science Foundation of Liaoning Province, Joint Research Fund Liaoning-Shenyang National Laboratory for Materials Science (Grant 20180510038), DICP (DICP ZZBS201708, DICP ZZBS201802, DICP I202032), DICP&QIBEBT (Grant DICP&QIBEBT UN201702), Dalian National Laboratory For Clean Energy (DNL), CAS, DNL Cooperation Fund, CAS (DNL180310, DNL180308, DNL201912, and DNL201915), National Synchrotron Radiation Laboratory (KY2060000173) and the Fundamental Research Funds for the Central Universities (WK2060140026).

### Appendix A. Supporting information

Supplementary data associated with this article can be found in the online version at [doi:10.1016/j.nanoen.2020.105688](https://doi.org/10.1016/j.nanoen.2020.105688).

### References

- [1] J. Shi, S. Wang, X. Chen, Z. Chen, X. Du, T. Ni, Q. Wang, L. Ruan, W. Zeng, Z. Huang, *Adv. Energy Mater.* 9 (2019) 1901957.
- [2] U.K. Bhaskar, N. Banerjee, A. Abdollahi, Z. Wang, D.G. Schlom, G. Rijnders, G. Catalan, *Nat. Nanotechnol.* 11 (2016) 263–266.
- [3] Y. Lin, J. Chen, M.M. Tavakoli, Y. Gao, Y. Zhu, D. Zhang, M. Kam, Z. He, Z. Fan, *Adv. Mater.* 31 (2019), e1804285.
- [4] M.D. Manrique-Juarez, F. Mathieu, V. Shalabaeva, J. Cacheux, S. Rat, L. Nicu, T. Leichle, L. Salmon, G. Molnar, A. Bousseksou, *Angew. Chem. Int. Ed.* 56 (2017) 8074–8078.
- [5] C.L.P. Huang, S. Pinaud, K. Brousse, R. Laloo, V. Turq, M. Respaud, A. Demortière, B. Daffos, P.L. Taberna, B. Chaudret, Y. Gogotsi, P. Simon, *Science* 351 (2016) 691–695.
- [6] P. Zhang, F. Wang, M. Yu, X. Zhuang, X. Feng, *Chem. Soc. Rev.* 47 (2018) 7426–7451.
- [7] A. Chortos, J. Liu, Z. Bao, *Nat. Mater.* 15 (2016) 937–950.
- [8] J.W. Choi, D. Aurbach, *Nat. Rev. Mater.* 1 (2016) 16013.
- [9] M.F. El-Kady, R.B. Kaner, *Nat. Commun.* 4 (2013) 9.
- [10] M.F. El-Kady, M. Ihms, M. Li, J.Y. Hwang, M.F. Mousavi, L. Chaney, A.T. Lech, R. B. Kaner, *Proc. Natl. Acad. Sci.* 112 (2015) 4233–4238.
- [11] S.H. Zheng, Z.S. Wu, F. Zhou, X. Wang, J.M. Ma, C. Liu, Y.B. He, X.H. Bao, *Nano Energy* 51 (2018) 613–620.
- [12] N.A. Kyeremateng, R. Hahn, *ACS Energy Lett.* 3 (2018) 1172–1175.
- [13] W. Qi, J.G. Shapter, Q. Wu, T. Yin, G. Gao, D. Cui, *J. Mater. Chem. A* 5 (2017) 19521–19540.
- [14] L. Suo, O. Borodin, Y. Wang, X. Rong, W. Sun, X. Fan, S. Xu, M.A. Schroeder, A. V. Cresce, F. Wang, C. Yang, Y.-S. Hu, K. Xu, C. Wang, *Adv. Energy Mater.* 7 (2017), 1701189.
- [15] M.H. Lee, S.J. Kim, D. Chang, J. Kim, S. Moon, K. Oh, K.-Y. Park, W.M. Seong, H. Park, G. Kwon, B. Lee, K. Kang, *Mater. Today* 29 (2019) 26–35.
- [16] M.R. Lukatskaya, J.I. Feldblyum, D.G. Mackanic, F. Lissel, D.L. Michels, Y. Cui, Z. Bao, *Energy Environ. Sci.* 11 (2018) 2876–2883.

- [17] D.P. Leonard, Z. Wei, G. Chen, F. Du, X. Ji, *ACS Energy Lett.* 3 (2018) 373–374.
- [18] R.-S. Kühnel, D. Reber, C. Battaglia, *ACS Energy Lett.* 2 (2017) 2005–2006.
- [19] D. Bin, F. Wang, A.G. Tamirat, L. Suo, Y. Wang, C. Wang, Y. Xia, *Adv. Energy Mater.* 8 (2018), 1703008.
- [20] Y.Z. Feng, Q. Zhang, S. Liu, J. Liu, Z.L. Tao, J. Chen, *J. Mater. Chem. A* 7 (2019) 8122–8128.
- [21] S.R. Chen, J.M. Zheng, D.H. Mei, K.S. Han, M.H. Engelhard, W.G. Zhao, W. Xu, J. Liu, J.G. Zhang, *Adv. Mater.* 30 (2018) 7.
- [22] L.W. Jiang, Y.X. Lu, C.L. Zhao, L.L. Liu, J.N. Zhang, Q.Q. Zhang, X. Shen, J. M. Zhao, X.Q. Yu, H. Li, X.J. Huang, L.Q. Chen, Y.S. Hu, *Nat. Energy* 4 (2019) 495–503.
- [23] L. Suo, Y.S. Hu, H. Li, M. Armand, L. Chen, *Nat. Commun.* 4 (2013) 1481.
- [24] L. Suo, O. Borodin, W. Sun, X. Fan, C. Yang, F. Wang, T. Gao, Z. Ma, M. Schroeder, A. von Cresce, S.M. Russell, M. Armand, A. Angell, K. Xu, C. Wang, *Angew. Chem. Int. Ed.* 55 (2016) 7136–7141.
- [25] Q. Nian, J. Wang, S. Liu, T. Sun, S. Zheng, Y. Zhang, Z. Tao, J. Chen, *Angew. Chem. Int. Ed.* 58 (2019) 16994–16999.
- [26] Y. Xu, Q. Wei, C. Xu, Q. Li, Q. An, P. Zhang, J. Sheng, L. Zhou, L. Mai, *Adv. Energy Mater.* 6 (2016), 1600389.
- [27] Y. Jiang, X.F. Zhou, D.J. Li, X.L. Cheng, F.F. Liu, Y. Yu, *Adv. Energy Mater.* 8 (2018) 7.
- [28] Y. Fang, L. Xiao, J. Qian, Y. Cao, X. Ai, Y. Huang, H. Yang, *Adv. Energy Mater.* 6 (2016), 1502197.
- [29] Y. Wu, Y. Yu, *Energy Storage Mater.* 16 (2019) 323–343.
- [30] M. Liu, H. Ao, Y. Jin, Z. Hou, X. Zhang, Y. Zhu, Y. Qian, *Mater. Today Energy* 17 (2020), 100432.
- [31] D.J. Kim, Y.H. Jung, K.K. Bharathi, S.H. Je, D.K. Kim, A. Coskun, J.W. Choi, *Adv. Energy Mater.* 4 (2014), 1400133.
- [32] S. Li, Y.F. Dong, L. Xu, X. Xu, L. He, L.Q. Mai, *Adv. Mater.* 26 (2014) 3545–3553.
- [33] Y. Jiang, Y. Yao, J. Shi, L. Zeng, L. Gu, Y. Yu, *ChemNanoMat* 2 (2016) 726–731.
- [34] H. Xiao, Z.-S. Wu, F. Zhou, S. Zheng, D. Sui, Y. Chen, X. Bao, *Energy Storage Mater.* 13 (2018) 233–240.
- [35] H. Xiao, Z.S. Wu, L. Chen, F. Zhou, S. Zheng, W. Ren, H.M. Cheng, X. Bao, *ACS Nano* 11 (2017) 7284–7292.
- [36] F. Zhou, H. Huang, C. Xiao, S. Zheng, X. Shi, J. Qin, Q. Fu, X. Bao, X. Feng, K. Mullen, Z.S. Wu, *J. Am. Chem. Soc.* 140 (2018) 8198–8205.
- [37] Y. Jiang, Z. Yang, W. Li, L. Zeng, F. Pan, M. Wang, X. Wei, G. Hu, L. Gu, Y. Yu, *Adv. Energy Mater.* 5 (2015), 1402104.
- [38] E. Brini, C.J. Fennell, M. Fernandez-Serra, B. Hribar-Lee, M. Luksic, K.A. Dill, *Chem. Rev.* 117 (2017) 12385–12414.
- [39] Q. Dou, Y. Lu, L. Su, X. Zhang, S. Lei, X. Bu, L. Liu, D. Xiao, J. Chen, S. Shi, X. Yan, *Energy Storage Mater.* 23 (2019) 603–609.
- [40] X. Bu, L. Su, Q. Dou, S. Lei, X. Yan, *J. Mater. Chem. A* 7 (2019) 7541–7547.
- [41] G.Q. Sun, H.S. Yang, G.F. Zhang, J. Gao, X.T. Jin, Y. Zhao, L. Jiang, L.T. Qu, *Energy Environ. Sci.* 11 (2018) 3367–3374.
- [42] C. Zeng, F. Xie, X. Yang, M. Jaroniec, L. Zhang, S.Z. Qiao, *Angew. Chem. Int. Ed.* 57 (2018) 8540–8544.
- [43] M.F. El-Kady, V. Strong, S. Dubin, R.B. Kaner, *Science* 335 (2012) 1326–1330.
- [44] T. Brezesinski, J. Wang, S.H. Tolbert, B. Dunn, *Nat. Mater.* 9 (2010) 146–151.
- [45] T. Brezesinski, J. Wang, J. Polleux, B. Dunn, S.H. Tolbert, *J. Am. Chem. Soc.* 131 (2009) 1802–1809.
- [46] S. Islam, M.H. Alfaruqi, D.Y. Putro, V. Mathew, S. Kim, J. Jo, S. Kim, Y.K. Sun, K. Kim, J. Kim, *ChemSusChem* 11 (2018) 2239–2247.
- [47] X. Zhang, X. Rui, D. Chen, H. Tan, D. Yang, S. Huang, Y. Yu, *Nanoscale* 11 (2019) 2556–2576.
- [48] F. Mo, G. Liang, Q. Meng, Z. Liu, H. Li, J. Fan, C. Zhi, *Energy Environ. Sci.* 12 (2019) 706–715.
- [49] S. Emamian, T. Lu, H. Kruse, H. Emamian, *J. Comput. Chem.* 40 (2019) 2868–2881.



**Xiao Wang** obtained B.S. degree in Material Chemistry from Shandong Agricultural University in 2016. She is pursuing the Ph.D. degree from Dalian Institute of Chemical Physics (DICP), Chinese Academy of Sciences (CAS), under the supervision of Prof. Zhong-Shuai Wu. Her research interests focus on graphene & 2D materials, flexible and planar electrochemical energy storage devices.



**Huijuan Huang** obtained B.S. degree in Materials Chemistry from University of Science and Technology of China (USTC) in 2018. She is a Ph.D. candidate in Department of Materials Science and Engineering, USTC, under the supervision of Prof. Yan Yu. Her research interests include the design and synthesis of functional carbon nanomaterials, design, synthesis and energy storage mechanism of electrode materials for high-performance sodium-ion batteries, potassium-ion batteries and potassium-selenium batteries.



**Shuanghao Zheng** received Ph.D. degree from DICP, CAS, under the supervision of Prof. Xinhe Bao and Prof. Zhong-Shuai Wu in 2019. Then, he was promoted to be associated professor at DICP, CAS. His research interests focus on graphene & 2D materials, planar and miniaturized electrochemical energy storage devices.



**Feng Zhou** received his Ph.D. degree from Lanzhou Institute of Chemical Physics, CAS in 2016. He currently works as a postdoctor at DICP, CAS, advised by Prof. Zhong-Shuai Wu. His research focuses on ionic liquids, graphene and 2D materials for supercapacitors & micro-supercapacitors.



**Pengfei Lu** received his Ph.D. degree from Yangzhou University in 2017. He worked as a postdoctor in DICP, CAS. His research focuses on DFT calculations and MD simulations of graphene and 2D materials for advanced energy storage devices, e.g., supercapacitors and Li-S batteries.



**Pratteek Das** received his MSc degree from the Indian Institute of Technology, Kharagpur in 2016. He worked on several projects on a wide range of topics like nanogenerators and crystallography in India, China and Germany before joining the 2D Materials & Energy Devices group at the Dalian Institute of Chemical Physics, CAS in 2017 as a PhD student, supervised by Prof. Zhong-Shuai Wu, under the sponsorship of CASTWAS President's Fellowship. His research interest involves the preparation and application of 2D heterostructures for energy storage devices like batteries and supercapacitors.



**Yan Yu** is a professor of material science at the University of Science and Technology of China (USTC). She received her Ph.D. in material science at USTC in 2006. From 2007–2008, she worked as a postdoctoral researcher at Florida International University. She worked at the Max Planck Institute for Solid-State Research in Stuttgart, Germany. Her current research interests mainly include the design of novel nanomaterials for clean energy, especially for batteries and the fundamental science of energy storage systems.



**Pengchao Wen** received his BS degree in the school of Materials Science and Engineering from Shaanxi University of Science and Technology and his Ph.D. in the school of Chemistry and Materials Science from University of Science and Technology of China in 2012, 2017 respectively. He currently works as a postdoctor at DICP, CAS, advised by Prof. Zhong-Shuai Wu. His research focuses on the 2D materials for high-energy and solid-state batteries.



**Zhong-Shuai Wu** received his Ph.D. from the Institute for Metal Research, CAS, in 2011 and worked as a postdoctoral fellow at the Max Planck Institute for Polymer Research in Mainz, Germany, from 2011 to 2015. Subsequently, Dr. Wu became a full professor and group leader of 2D materials chemistry & energy applications at DICP, CAS, and was promoted in 2018 as a DICP Chair Professor. Currently, Dr. Wu's research interests include graphene and 2D materials, surface- and nanoelectrochemistry, microscale electrochemical energy storage devices, supercapacitors, batteries and catalysts.